ARTICLE   OPEN

Single-stage tubular and multistage planar systems of passive permeate-side-heated solar membrane distillation

Shahin Ahmed Sujon[1] and Peng Yi [ID][1 ✉]

Scarcity of drinking water is a global problem and especially serious in rural areas of developing countries. Passive permeate-side-heated interfacial-heating solar membrane distillation has been shown recently as a promising system for off-grid distributed water and wastewater treatment. In this study, single-stage tubular systems were developed by giving the poly(vinylidene fluoride) (PVDF) membrane (pore size: 0.45 μm) a tubular structure with the outer surface (i.e., the permeate side) coated with carbon black NPs which absorbed solar thermal energy and evaporated the feedwater inside the membrane tube. Under natural sunlight, the vertical tubular system had a production rate of distilled water per footprint of 0.67–2.06 $kg\,m^{-2}\,day^{-1}$ throughout the year, 71% higher than the single-stage planar system on average. The three-stage planar systems were developed by overlapping three single-stage modules. Two adjacent modules shared a common copper sheet that serves as both the top of the condensation chamber of the preceding stage and the bottom of the feedwater chamber of the following stage. The copper sheet can partially transfer the condensation heat of the preceding stage to the feedwater of the following stage, thus enhancing the system energy efficiency (η_{sys}) in producing distilled water. The η_{sys} and distillate flux of the three-stage systems were 62% and 5.01 $kg\,m^{-2}\,day^{-1}$, respectively, at the average daytime irradiance of 422 $W\,m^{-2}$, 34% higher than the single-stage planar systems.

INTRODUCTION

Water is an invaluable resource for human being. However, due to the rapid growth of population and overuse of water resources, it is estimated that 1.8 billion people will live with water scarcity by 2025[1]. Most of them live in the rural areas of developing countries and are often forced to drink unclean water[2], which can lead to water-borne diseases or death[3]. In addition, people may also experience a temporary shortage of drinking water in disaster situations. For example, in July 2007, the flash flood in Gloucestershire, United Kingdom left 140,000 homes without drinking water for 17 days[4]. In February 2010, the tsunami caused by an earthquake in Southern Chile affected 70% of the Chilean population[5], and interrupted the supply of electricity and water for several days[6]. Therefore, affordable water purification systems that require no electrical energy are crucial for water-stressed and disaster-prone areas.

Since most of the regions facing water scarcity (e.g., Northwestern China[7], Southwestern U.S.[8], Northwestern Bangladesh[9], West Asia, sub-Saharan Africa[10]) have high solar radiant exposure, solar interfacial distillation is a promising technology for off-grid water production. Following the pioneering works of Wang's[11] and Chen's[12] groups, researchers continued inventing novel photothermal materials and let them float on water surface to enhance evaporation energy efficiency (η_{evp}). Some examples in recent two years are Ti^{3+}-doped TiO_2 ($\eta_{evp} = 77.1\%$)[13] and silver/polypyrrole ($\eta_{evp} = 92.6\%$)[14] on the floats of hydrophilic cellulose membranes, marine biomass-derived hydrophilic aerogels with polyaniline nanoparticles as solar absorber ($\eta_{evp} = 88\%$)[15], a porous hydrophilic polyimide foam with a carbonized top ($\eta_{evp} = 83.2\%$)[16], WO_{3-x} microrods supported by a 0.5 cm-thick basswood float ($\eta_{evp} = 82.5\%$)[17], and carbonized Fe_3O_4-modified cellulose with hydrophilic external surface ($\eta_{evp} = 71.8\%$)[18], all under one sun, i.e., 1.0 $kW\,m^{-2}$. The η_{evp} was calculated by dividing the total enthalpy of vaporization of evaporated water (in

some cases sensible heat was also included) by the total radiant energy received on the surface of photothermal floats.

Several groups utilized photothermal floats in the distillation systems that include both evaporation and condensation processes to produce distilled water[19–21]. However, few researchers quantified the system energy efficiency in producing distilled water (η_{sys}), which can be calculated by dividing the total enthalpy of vaporization of the produced distilled water by the total radiant energy received by the surface of photothermal floats (often replaced by the global horizontal solar radiant exposure times the area of photothermal floats since the actual received radiant energy within the system was difficult to measure). The most recent example is a solar desalination system that used carbon black-coated aluminum plate to heat the feedwater wicked by a fiber cloth under the aluminum plate[22]. Its η_{sys} was reported as 24%[22]. A previous example is a system using floating polystyrene bars wrapped by hydrophilic cellulose fabric ($\eta_{sys} = 24\%$)[23]. One limitation of photothermal floats is that one cannot tilt the system and let the surface of solar absorber receive a higher irradiance than the horizontal plane[24].

In addition to hydrophilic photothermal floats, hydrophobic membranes coated or integrated with photothermal materials were employed for interfacial distillation. Instead of floating on the free surface of water, hydrophobic membranes were used to contain and heat the feedwater in interfacial-heating solar membrane distillation (ISMD) systems. In feed-side-heated ISMD, the feed side of the membrane was coated with photothermal materials (e.g., silver[25], carbon black[26], titanium nitride nanoparticles[27], and polydopamine[28,29]) for absorbing solar thermal energy and heating the feedwater at the air-water interface which is also the membrane-water interface. In many studies on active ISMD, the system energy efficiency in producing distilled water (η_{sys}) was overestimated because the electrical energy consumed by the peristaltic pumps for circulating the feedwater, distilled

---

[1]Department of Civil, Environmental and Geomatics Engineering, Florida Atlantic University, Boca Raton, FL 33431-0991, USA. ✉email: pyi@fau.edu
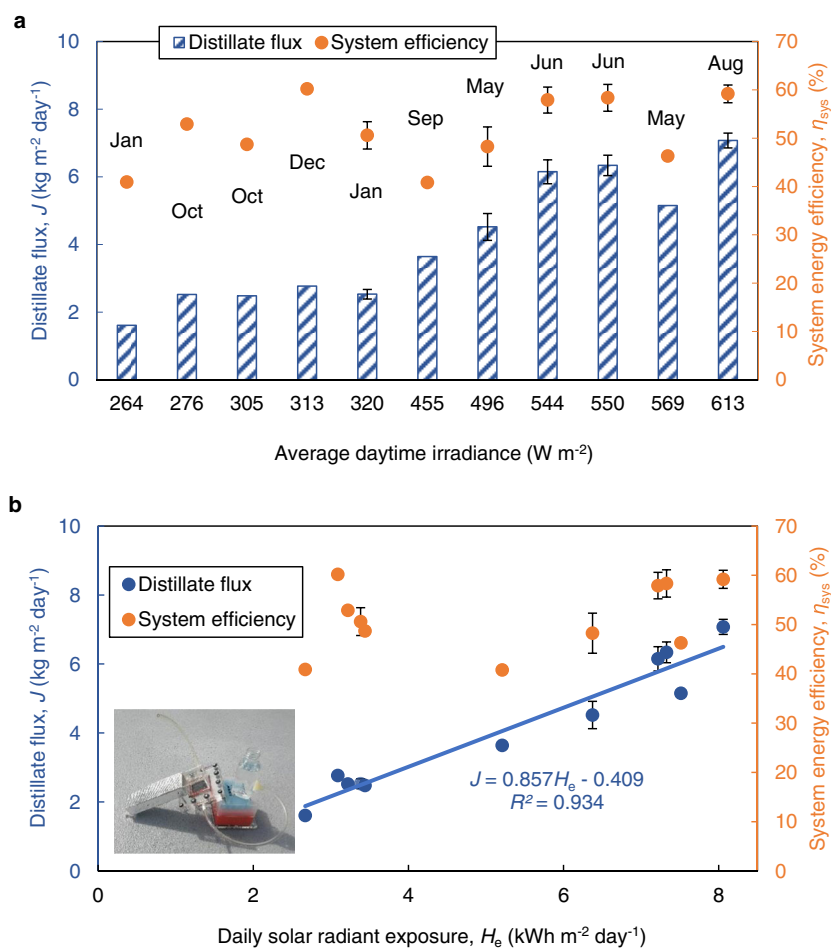
npj

Fig. 1 The performance of single-stage planar systems under natural sunlight. a Distillate production rates per unit area of black membrane (i.e., distillate fluxes, J) and the corresponding system energy efficiencies, η_{sys}, of the single-stage planar system (membrane dimensions: 50 mm × 50 mm) under natural sunlight in different months at different average daytime irradiances. **b** Distillate production fluxes and the corresponding energy efficiencies with respect to daily solar radiant exposure, H_e, for the same experiments presented in **a**. The inset of Fig. 1b is the photograph of a single-stage planar system. The systems were placed at an inclination of 30° with respect to the horizontal, facing south under natural sunlight from sunrise to sunset during experiments. The surface density of carbon black NPs on the permeate side of PVDF membranes (pore size: 0.45 μm) was 7.5–7.9 g m^{-2} and the hydrostatic pressure at the center of the membrane was 95–105 mmH$_2$O (i.e., 0.93–1.03 kPa), as shown in Supplementary Table 2. DI water was used as feedwater in these experiments, during which the temperature of feedwater was within 16–38 °C. Variation in irradiance and weather condition can be found in Supplementary Table 1. The error bars represent the standard deviations of duplicate results obtained using two different systems on the same day.

water, or both was not considered. In a passive feed-side-heated ISMD system using polydimethylsiloxane/carbon nanotube/poly(-vinylidene fluoride) (PDMS/CNT/PVDF) membrane, the production flux of distilled water was 0.9 kg m^{-2} h^{-1} and the η_{sys} was 60% under one sun [30].

Our group recently invented a passive permeate-side-heated ISMD[24]. It was also the first permeate-side-heated MD system. The permeate side of the hydrophobic membrane (i.e., 0.45 μm PVDF membrane) was coated with carbon black NPs, which absorbed solar thermal energy and transferred the heat to the feedwater that was in contact with the feed side of the membrane. Unlike the feed-side-heated ISMD in which sunlight has to pass through feedwater, sunlight only needs to pass through the air in the distillation chamber before reaching the photothermal coating in the permeate-side-heated ISMD, resulting in less attenuation and higher η_{sys}. Compared to the horizontal photothermal floats, the permeate-side-heated ISMD can be placed at an inclination to receive a higher irradiance[24]. The system produced a distillate flux of 8.56 kg m^{-2} day^{-1} at an average daytime irradiance of 652 W m^{-2} which corresponds to an η_{sys} of 67.5%, the highest single-stage η_{sys} under natural sunlight to the best of our

knowledge among all published solar distillation systems. The initial distillate flux was independent of the type of feedwater (i.e., deionized (DI) water, seawater, canal water, and municipal wastewater). It was the first interfacial distillation system that demonstrated the ability to extract potable water directly from municipal wastewater.

One advantage of membrane distillation lies in its flexibility in increasing the area of air–water interface in a given space by containing the feedwater within a designed geometry of hydrophobic membranes. In this study, tubular permeate-side-heated ISMD systems have been developed to contain the feedwater in tubular hydrophobic membranes and increase the production rate of distilled water per unit footprint area under natural sunlight. It is the first 3D design of interfacial-heating membrane distillation. The relationship between the daily solar radiant exposure and distillate flux has been derived for tubular systems in comparison with that of planar systems. In addition, multistage (e.g., three-stage) planar permeate-side-heated ISMD systems have been built to increase the η_{sys} of planar systems under natural sunlight through partially recovering the heat of condensation.

RESULTS AND DISCUSSION

System energy efficiency (η_{sys}) and distillate flux of single-stage planar permeate-side-heated ISMD systems at different solar radiant exposures

The single-stage planar system (the inset in Fig. 1b) developed in our previous study[24] was thoroughly tested under natural sunlight at different average daytime irradiances in various months to measure the η_{sys} and distillate flux of the system (Fig. 1a). The inner dimensions of feedwater chamber, transparent distillation chamber and condensation chamber are 50 mm (L) × 50 mm (W) × 14 mm (H), the upper distillation chamber above the flange: 60 mm (L) × 60 mm (W) × 40 mm (H); the lower distillation chamber within the flange: 50 mm (L) × 50 mm (W) × 14 mm (H), and 207 mm (L) × 60 mm (W) × 30 mm (H), respectively. All the experiments were conducted at an inclination of 30° with respect to the horizontal with the membrane facing south from sunrise to sunset on either a fully or partly sunny day, during which the variation of irradiance can be found in Supplementary Table 1. Other experimental details such as surface density of carbon black on the permeate side of membrane, hydrostatic pressure at the center of membrane, and the temperature of feedwater (i.e., DI water) can be found in Supplementary Table 2.

At the end of the distillation experiments, the condensed water was collected and weighed and the distillate production rate per unit area of the membrane (i.e., the distillate flux) was calculated by dividing the mass of distilled water by the area of membrane (i.e., 50 mm × 50 mm). The system energy efficiency (η_{sys}) was calculated using the following equation[23,24]:

$$\eta_{sys} = \frac{\Delta H_{vap} \times M_w}{E_e \times t} \qquad (1)$$

where ΔH_{vap} is the enthalpy of water vaporization (kJ kg^{-1})[31] at the average temperature of feedwater during experiments, M_w is the mass of distilled water produced per unit area of black membrane (kg m^{-2}), E_e is the average of global horizontal irradiance of sunlight (kW m^{-2}) that was measured every 30 s during the experiments from sunrise to sunset, t is the duration of the experiments (second). Since it is almost impossible to measure the actual irradiance received by the solar thermal collector (i.e., the black permeate side of membrane in this study) in an enclosed

system, it is a common practice to measure the global horizontal irradiance instead. Thus, the η_{sys} obtained from Eq. 1 provides a fair comparison on the efficiencies of different systems in producing distilled water under the same ambient solar irradiance.

The η_{sys} and distillate flux of the single-stage planar system were 41–60% and 1.61–7.08 kg m^{-2} day^{-1}, respectively, in the experiments conducted throughout the year (Fig. 1a). There was no obvious dependence of η_{sys} on the average daytime irradiance or season possibly because all the experiments were conducted on sunny days. Our previous study[24] showed that η_{sys} more strongly depends on the weather condition than the irradiance or season. As a result, the distillate flux increased with increasing irradiance in Fig. 1a. In Fig. 1b, the distillate fluxes and system energy efficiencies of the same experiments were plotted as a function of daily solar radiant exposure, H_e (kWh m^{-2} day^{-1}) that is equal to $E_e \times t$ in Eq. 1. The η_{sys} is independent of H_e whereas distillate flux J (kg m^{-2} day^{-1}) linearly increases with increasing H_e. The linear least squares regression between J and H_e shows that $J = 0.857 H_e − 0.409$ with the square of correlation coefficient (R^2) as 0.934. Thus, one can use this equation to estimate the distillate flux on sunny days based on the measured daily radiant exposure for the same system facing south at 30° inclination with respect to the horizontal at the same location and maybe at the locations with the same latitude as well. It requires further studies to know whether this equation applies to other locations or not. The negative y intercept suggests that the system will only start producing distilled water when the daily radiant exposure is higher than a certain threshold value.

Tubular permeate-side-heated ISMD system

In order to reduce the footprint of solar distillation, a single-stage tubular passive permeate-side-heated interfacial-heating solar membrane distillation system has been developed (Fig. 2). In this tubular system, the upper part is the transparent distillation chamber and the lower part is the condensation chamber. A hydrophobic microporous membrane was given a tubular shape by jointing the two edges of the membrane and placed at the center of the distillation chamber. The feedwater filled the inside of the membrane tube by gravity from an elevated reservoir. Due to the hydrophobicity of the membrane, the feedwater cannot
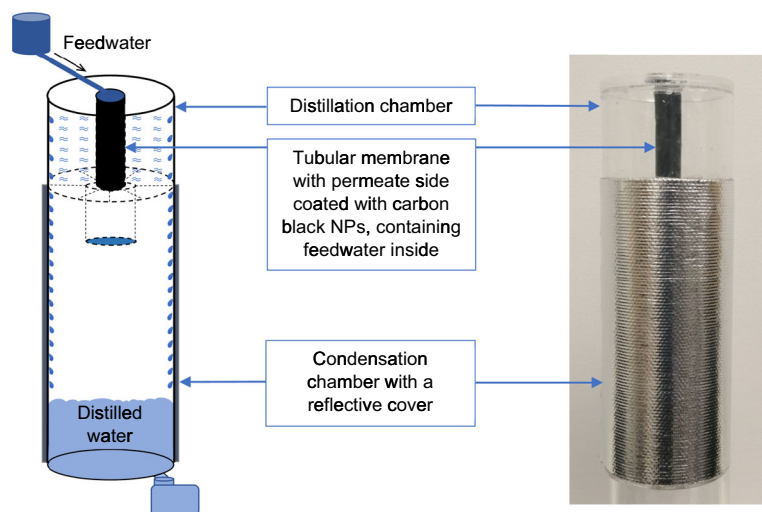

Fig. 2 The schematic and photograph of the tubular passive permeate-side-heated solar membrane distillation system. The tubular system was placed vertically during operation. The inner dimensions of this system are as follows: feedwater chamber (i.e., inside of the tubular membrane) [50 mm (H), 16 mm (D)], distillation chamber [50 mm (H), 70 mm (D)], condensation chamber [158 mm (H), 70 mm (D)]. The tubular membrane had the dimensions of 50 mm × 50 mm before rolling. The volume of the distillation chamber and the inner surface area of the condensation chamber of the tubular system were the same as those of the planar system shown in Fig. 1. In addition, there was a container right below the tubular membrane to contain water leaks in case there was any. However, no leaking of feedwater was observed in the experiments reported in this study.
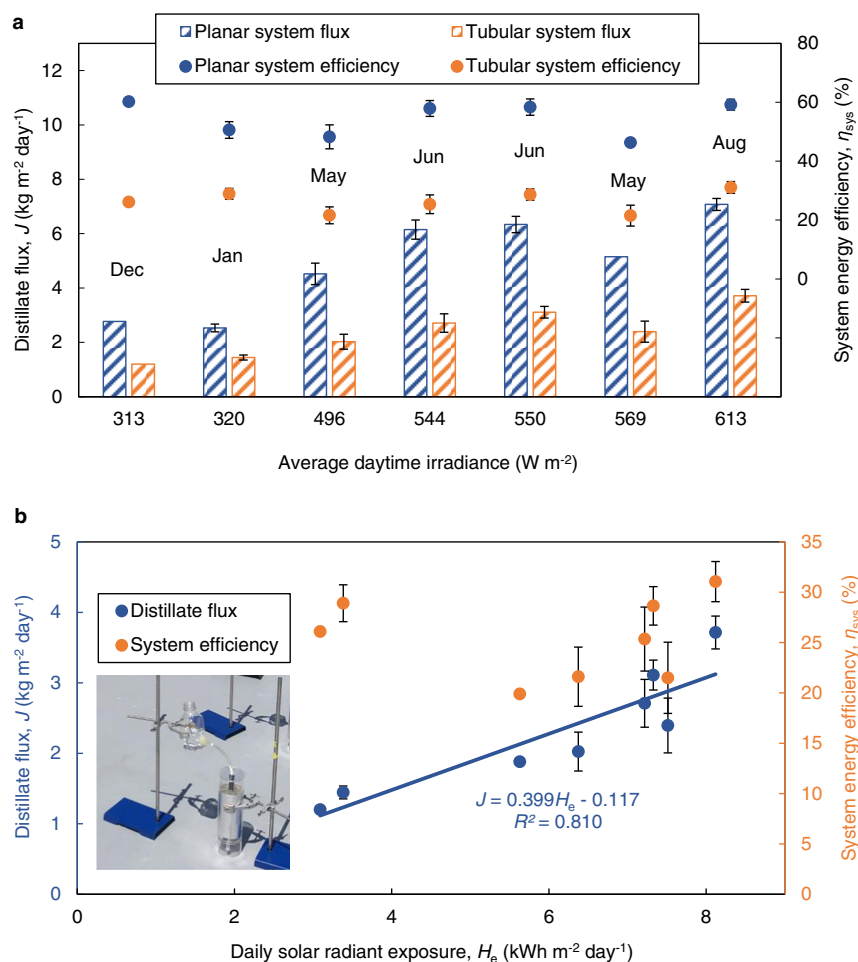
Fig. 3 The performance of single-stage tubular systems under natural sunlight. a Distillate production rates of tubular systems per unit area of black membrane (i.e., distillate flux, J) and the system energy efficiencies, η_{sys}, under natural sunlight (from sunrise to sunset) in various months of a year at different solar irradiances, in comparison with that of planar systems at 30° inclination to the ground. Both systems had the same membrane dimensions (i.e., 50 mm × 50 mm). The data of single-stage planar systems were copied from Fig. 1a for convenient comparison with tubular systems. **b** Distillate fluxes and system energy efficiencies of tubular systems with respect to daily solar radiant exposure, H_e, calculated based on the global horizontal irradiance. The surface density of carbon black NPs on the permeate side of PVDF membrane (pore size: 0.45 µm) was 7.5–7.9 g m^{-2} and the hydrostatic pressure on the center of the membrane was 90–105 mmH$_2$O (i.e., 0.88–1.03 kPa) for both tubular and planar systems, as shown in Supplementary Table 3. DI water was used as feedwater in the experiments, and the temperature of feedwater was between 22 and 36 °C. Variations in irradiance and weather condition can be found in Supplementary Table 1. The error bars represent the standard deviations of duplicate results obtained using two different systems on the same day.

penetrate the membrane tube and the inside of the membrane tube is essentially a feedwater chamber. The outer surface of the membrane tube was coated with carbon black nanoparticles, which absorbed solar radiation and converted the radiation to heat. The heat was transferred through conduction[24] to the feedwater that partially entered the capillary pores of the membrane from the inside of the membrane tube. Thus, the feedwater was effectively evaporated through interfacial heating. Upon evaporation, water vapor passed through the pores of the membrane and entered the tubular transparent distillation chamber that contained the membrane tube and the steam. The outer surface of the condensation chamber was covered by a reflective heat barrier that reflected the sunlight and helped keep the inside of the chamber cool where water vapor condensed into distilled water. The tubular system was set vertically so that the distilled water was collected at the bottom of the system.

The performance of the tubular system was compared with the single-stage planar system after they were tested simultaneously under natural sunlight from sunrise to sunset at the same locations. The two systems used the same type and size of membrane, i.e., PVDF membrane with a nominal pore size of

0.45 µm and dimensions of 50 mm × 50 mm. Thus, the tubular membrane has a diameter of 16 mm and a height of 50 mm. The distillation chamber of the tubular system has an inner diameter of 70 mm and a height of 50 mm, which gives about the same volume (difference within 2%) as the distillation chamber of the planar system. Therefore, the water vapor had the same room to flow into the condensation chambers in both systems. The acrylic glass tube also has the same thickness (1/8 inch) as the distillation chamber of the planar system. The condensation chamber of the tubular system has an inner diameter of 70 mm and a height of 158 mm. The inner surface areas of the condensation chambers in both systems were about the same (difference within 2%) on which the water vapor condensed to distilled water. Other experimental details such as surface density of carbon black on the permeate side of membranes, hydrostatic pressure at the center of membranes, and feedwater (i.e., DI water) temperature for both systems are presented in Supplementary Table 3. The variation of solar irradiance during experiments can be found in Supplementary Table 1.

As presented in Fig. 3a, the η_{sys} and the distillate production rate per unit area of membrane (i.e., distillate flux) of the tubular

system were 20–31% and 1.20–3.72 kg m^{-2} day^{-1}, respectively, which are 48 ± 5% (ave. ± std. dev.) of that of single-stage planar systems at 30° inclination with respect to the horizontal despite the season or irradiance. This is probably due to that only half of the tubular membrane can receive direct solar radiation whereas the entire membrane in the planar system can receive direct solar radiation. These results also suggest that diffuse solar radiation does not play an important role in distilled water production in permeate-side-heated ISMD. However, compared to the same planar system facing south at 90° inclination (Supplementary Figure 1), both the η_{sys} and distillate flux of the tubular system were 69% higher than the vertical planar system likely because the tubular system can receive direct solar radiation from any direction throughout the day whereas the vertical planar system can only receive direct solar radiation from the south. In Fig. 3b, the distillate flux, J (kg m^{-2} day^{-1}), and system energy efficiency, η_{sys}, of the tubular system were plotted as a function of daily solar radiant exposure, H_e (i.e., $E_e \times t$), in kWh m^{-2} day^{-1}. The η_{sys} does not clearly depend on H_e. The linear least squares regression between J and H_e shows that $J = 0.399\ H_e$–0.117 with the square of correlation coefficient (R^2) as 0.810.

By design, the vertical tubular system has a much smaller footprint (0.0045 m^2) than that of planar system at 30° inclination (0.016 m^2 without consideration of the flange) and could be a better option where land is precious. Figure 4 compares the production rate of distilled water per unit area of footprint between the single-stage planar and the tubular systems under natural sunlight using the same experiments presented in Fig. 3a. The production rate per footprint of the tubular system was 0.67–2.06 kg m^{-2} day^{-1}, on average 71 ± 18% (ave. ± std. dev.) higher than that of the planar system facing south at 30° inclination (i.e., 0.40–1.11 kg m^{-2} day^{-1}). In addition, the tubular system is expected to increase its production rate without changing its footprint by simply increasing the height of the membrane tube and the tubular distillation chamber.

Multistage planar passive permeate-side-heated ISMD system

In order to improve the distillate flux and system energy efficiency of the planar system through enhanced evaporation and condensation, a three-stage planar permeate-side-heated solar
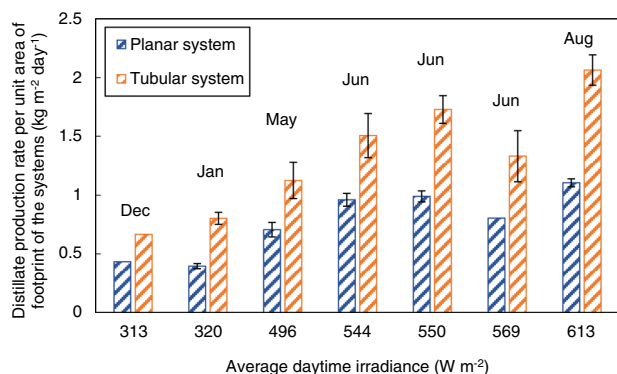

Fig. 4 Distillate production rates of single-stage planar and tubular systems per unit area of footprint under natural sunlight. Both the planar and tubular systems had the same membrane dimensions (i.e., 50 mm × 50 mm), the same volume of distillation chamber, and the same inner surface area of the condensation chamber. The surface density of carbon black NPs on the permeate side of the membrane was 7.5–7.9 g m^{-2} and the hydrostatic pressure at the center of the membranes during the experiment ranged between 90 and 105 mmH$_2$O (i.e., 0.88 and 1.03 kPa), as shown in Supplementary Table 3. Variations of irradiance and weather condition can be found in Supplementary Table 1. The error bars represent the standard deviations of duplicate results obtained using two different systems on the same day.

membrane distillation system has been developed as shown in Fig. 5. Each stage has a feedwater chamber [120 mm (L) × 50 mm (W) × 14 mm (H)], a transparent distillation chamber [the upper distillation chamber above the flange: 130 mm (L) × 60 mm (W) × 40 mm (H); the lower distillation chamber within the flange: 120 mm (L) × 50 mm (W) × 14 mm (H)], and a condensation chamber [150 mm (L) × 60 mm (W) × 30 mm (H)]. A hydrophobic 0.45 μm PVDF membrane [120 mm (L) × 50 mm (W)], with the permeate side coated with carbon black NPs, is placed between each stage's distillation and feedwater chambers with gaskets on both sides of the membrane. Two adjacent stages share a common copper sheet [150 mm (L) × 67 mm (W) × 4 mm (H)] that serves as both the top of the condensation chamber of the preceding stage and the bottom of the feedwater chamber of the following stage (i.e., between 1st and 2nd, and between 2nd and 3rd stage as presented in Fig. 5).

Feedwater (i.e., DI water) filled the feedwater chamber of each stage from respective elevated reservoirs. Due to the hydrophobicity of the PVDF membrane and the capillary effect, the feedwater cannot penetrate the membrane. Sunlight passed through the transparent distillation chambers and reached the black permeate side of the membranes. The absorbed heat was transferred to the feedwater on the feed side of the membrane through conduction resulting in interfacial heating and evaporation. The water vapor passed through the pores of the membranes and entered the condensation chambers due to the vapor pressure gradient between the heated air–water interface within the membrane and the cooler condensation chambers[24], where the water vapor condensed into distilled water. The copper sheet at the top of the condensation chamber of the preceding stage can easily transfer the condensation heat to the feedwater chamber of the following stage, due to its high thermal conductivity (400 W m^{-1} K^{-1})[32]. The recovery of condensation heat can enhance the evaporation of feedwater in the following stage, while the cooler temperature of feedwater can accelerate the condensation process in the preceding stage.

The three-stage planar systems were tested under natural sunlight from sunrise to sunset on two different sunny days in August 2021, along with control experiments using the single-stage planar systems with the identical dimensions of membrane [i.e., 120 mm (L) × 50 mm (W)], feedwater chamber, distillation chamber and condensation chamber as the three-stage systems, both facing south at 30° inclination with respect to the horizontal (Fig. 6a). The variation of solar irradiance during the experiments can be found in Supplementary Table 4. Other experimental details such as surface density of carbon black on the permeate side of 0.45 μm PVDF membrane, hydrostatic pressure on the membranes, and temperature of feedwater (i.e., DI water) are summarized in Supplementary Table 5. As shown in Fig. 6b, the system energy efficiency, η_{sys}, and distillate production rate per unit area of membrane (i.e., distillate flux, J) of the three-stage systems were 62% and 5.01 kg m^{-2} day^{-1} at the average daytime irradiance of 422 W m^{-2}, and 60% and 6.17 kg m^{-2} day^{-1} at 551 W m^{-2}, respectively. The η_{sys} and J of the three-stage systems were 34% and 37% higher than that of the single-stage systems at 422 W m^{-2} and 551 W m^{-2}, respectively, due to both enhanced condensation through the cooling of the condensation chamber by the feedwater of the next stage and enhanced evaporation through the recovery of condensation heat from the condensation chamber of the preceding stage.

The specific roles of enhanced condensation and enhanced evaporation in improving the η_{sys} and J of the three-stage systems are elucidated by analyzing the η_{sys} and J of each stage in comparison with the single-stage data. The 1st stage only had enhanced condensation; the 3rd stage only had enhanced evaporation; the 2nd stage had both. At 422 W m^{-2} (Fig. 6c), the enhanced condensation in 1st stage resulted in 22% increase in η_{sys} and J compared to the single-stage; the enhanced
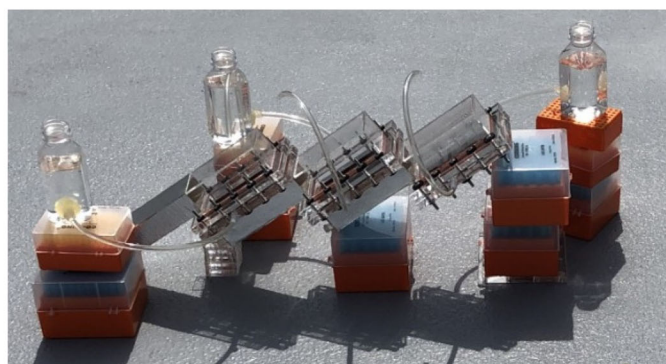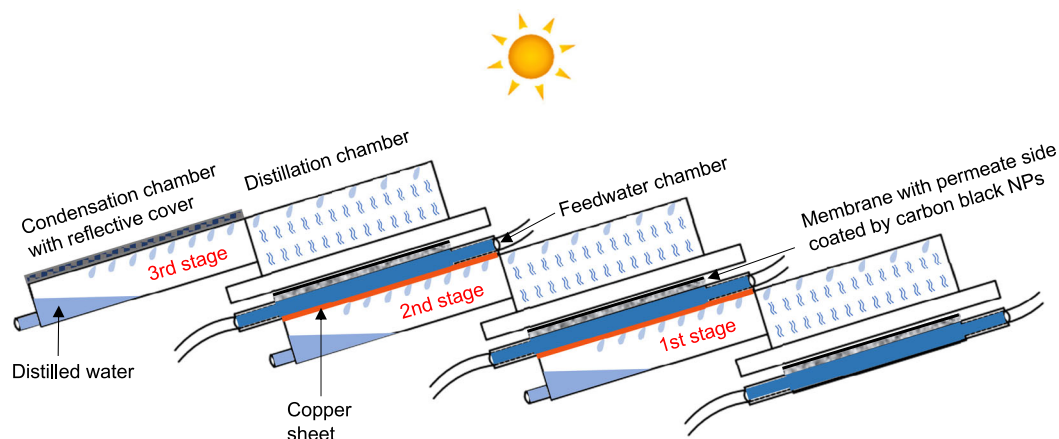
Fig. 5 The schematic and photograph of the three-stage planar passive permeate-side-heated solar membrane distillation system. The inner dimensions of different chambers of this three-stage planar system were as follows: feedwater chamber [120 mm (L) × 50 mm (W) × 14 mm (H)], distillation chamber [the upper distillation chamber above the flange: 130 mm (L) × 60 mm (W) × 40 mm (H); the lower distillation chamber within the flange: 120 mm (L) × 50 mm (W) × 14 mm (H)], and condensation chamber [150 mm (L) × 60 mm (W) × 30 mm (H)]. The dimensions of membranes were 120 mm (L) × 50 mm (W), and the dimensions of copper sheets were 150 mm (L) × 67 mm (W) × 4 mm (H). The copper sheets served as both the top of the condensation chamber of the preceding stage and the bottom of the feedwater chamber of the following stage for readily transferring the heat of condensation from the condensation chamber to the feedwater.

evaporation in 3rd stage resulted in 39% increase; the combination of both enhanced condensation and evaporation in 2nd stage resulted in 42% increase; the average is the 34% increase by the entire three-stage system. The highest η_{sys} (i.e., 66%) and J (i.e., 5.30 kg m^{-2} day^{-1}) were found in the 2nd stage. Similarly, at 551 W m^{-2} (Supplementary Fig. 2), the enhanced condensation in 1st stage resulted in 20% increase in η_{sys} and J compared to the single-stage; the enhanced evaporation in 3rd stage resulted in 43% increase; the combination of both enhanced condensation and evaporation in 2nd stage resulted in 47% increase; the average is the 37% increase by the entire three-stage system. The highest η_{sys} (i.e., 64%) and J (i.e., 6.64 kg m^{-2} day^{-1}) were found in the 2nd stage. This fact suggests that the η_{sys} and J of a multistage planar system should increase with the total number of stages even though such increase will become negligible when the number of stages is large.

In addition, the distillate production rates per unit area of footprint of three-stage systems were 2.67 and 3.30 kg m^{-2} day^{-1} at 422 and 551 W m^{-2}, respectively, 94% and 99% higher than that of single-stage systems (Fig. 6d), due to the overlap of the condensation chamber of the preceding stage with the feedwater chamber of the following stage. It is also much higher than that of tubular systems, i.e., 0.67–2.06 kg m^{-2} day^{-1} (Fig. 4).

Potential applications

The water intakes of male and female adults are on average 2.5 and 2 L day^{-1}, respectively, under sedentary condition[33,34], and can approach 6 L day^{-1} if active in a warm environment[34]. The residential water demand in the rural areas of developing countries was reported as 87, 25–29, 46–71, and 117 L per capita per day in Bangladesh (Dorogram village of Manikganj district)[35], Benin[36], China (Wei River Basin)[37], and India (Hisar District of Haryana)[38], respectively. The demand (e.g., uses for clothes washer, shower, tap, dishwasher, bathtub, toilet, irrigation, leak, etc.) increases to 120–650 L per capita per day in developed countries based on the data from Australia, Denmark, New Zealand, Poland, UK, and USA in 1992–2007[39,40]. The distillate production rate per unit area of membrane (i.e., distillate flux) of planar and tubular systems measured in this study were 1.61–7.08 kg m^{-2} day^{-1} and 1.20–3.72 kg m^{-2} day^{-1}, respectively, depending on the daytime irradiance. Thus, one sedentary adult would need to have a planar or tubular system with a membrane area of at least 1.6 or 2.1 m^2, respectively, to produce enough potable water throughout the year at the latitude close to or lower than that of Florida Atlantic University (FAU) (i.e., 26°22′19″N). If the adult is physically active, the membrane area needed for drinking water production would be 3.8 and 5.0 m^2 for planar and tubular systems, respectively. If the household resides in rural or remote areas where land is inexpensive, several arrays of
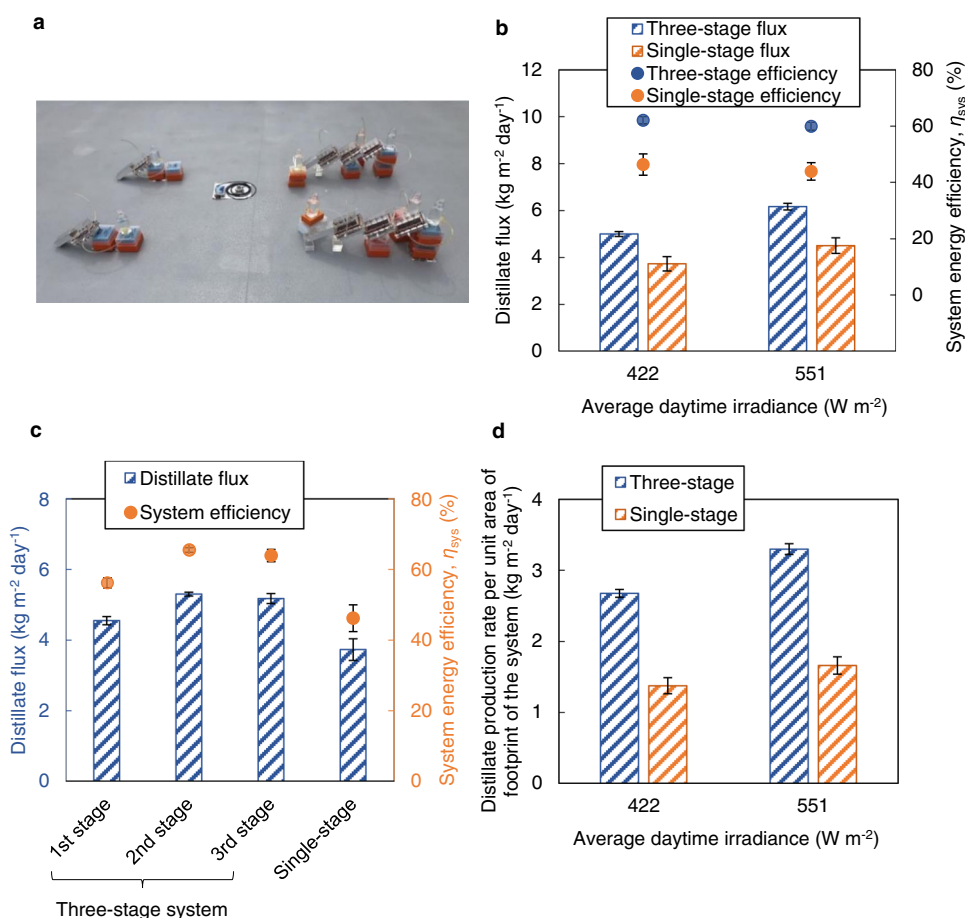
Fig. 6 The performance of three-stage planar systems under natural sunlight. a The photograph of three-stage and single-stage planar systems [membrane dimensions: 120 mm (L) × 50 mm (W)] placed under natural sunlight at 30° inclination with respect to the horizontal. **b** Distillate fluxes and system energy efficiencies of three-stage systems compared with that of single-stage planar systems under natural sunlight in August, 2021. The single-stage systems had the same dimensions as each stage in the three-stage systems. **c** Distillate fluxes and efficiencies in each stage of the three-stage systems, and the single-stage planar systems at an average daytime irradiance of 422 W m^{-2}. **d** Distillate production rate of the single-stage and three-stage planar systems under natural sunlight per unit area of footprint. The surface density of carbon black NPs on the permeate side of membrane was 7.1–8.0 g m^{-2} and the hydrostatic pressure at the center of the membrane was 95–105 mmH$_2$O (0.93–1.03 kPa), for both systems, as shown in Supplementary Table 5. In these experiments, DI water was used as feedwater and feedwater temperature was between 22.5 and 33 °C. Variation of irradiance and weather condition can be found in Supplementary Table 4. The error bars represent the standard deviations of duplicate results obtained using two different systems on the same day.

permeate-side-heated ISMD systems can be installed to help meet the residential water needs.

METHODS

Materials and equipment

The main structure of tubular and planar systems were constructed using transparent poly(methyl methacrylate) (PMMA) sheets, tubes, or both. PMMA tubes had a thickness of 1/8 inch and an inner diameter of 70 mm. PMMA sheets had a thickness of 1/8 or 1/2 inch. Pure copper sheets (SQINAA™, thickness: 4 mm) were used in the three-stage systems between the condensation chamber in the preceding stage and the feedwater chamber in the following stage (Fig. 5). Sealing gaskets for planar systems were made of silicone rubber (Grainger®, item No. 1MWF2). In order to join the pieces of plexiglasses and the two edges of the membrane for giving it a tubular shape, an acrylic plastic cement (SCIGRIP® 10315 16) was used. The condensation chambers were covered by aluminized reflective heat barriers (Thermo-Tec®, Part No. 13575).

PVDF flat-sheet membranes (Thermo Scientific™, Catalog No. 88518, pore size: 0.45 μm) were used in both tubular and planar systems. The thickness of the membrane was measured as 75–80 μm in our previous study[24], and it was reported to have an average porosity of 74%[41]. The source of the coating of carbon black NPs was Speedball® super black ink which also contains 2-dimethylaminoethanol and aqueous borated shellac. For coating, 450 μL of the ink was spread very gently on the permeate side of the membrane using a glass tube. The membrane was weighed (using LF 224 R, Intelligent Weighing Technology) before and after coating in order to calculate the surface density of carbon black NPs.

DI water (Millipore, MA) was used as the feedwater in all experiments and had a resistivity of 18.2 MΩ·cm. The temperature of feedwater during experiments was measured every 2 h using a thermometer (VWR®, Catalog No. 89095-598).

A pyranometer (Hukseflux, LP02-LI19) was used to measure the irradiance of sunlight during the experiments. This pyranometer has a nominal spectral response for 285–3000 nm wavelength. The

data logger recorded the irradiance of sunlight every 30 seconds throughout the experiments.

Development of the tubular passive permeate-side-heated solar membrane distillation system

The main structure of the tubular system was built with a transparent PMMA tube (thickness: 1/8 inch; inner diameter: 70 mm). The tube has a transparent upper part (i.e., the distillation chamber) and a lower part (i.e., the condensation chamber) covered by the reflective heat barrier as shown in Fig. 2. The lengths of the transparent distillation chamber and the covered condensation chamber are 50 mm and 158 mm, respectively. The top of the system was made of two layers of PMMA disk (thickness: 1/8 inch; diameter: 76 mm) and the bottom of the system was made of one layer of such disk. There was a hole at the center of the top to allow the feedwater to flow from an elevated reservoir into the membrane tube (i.e., the feedwater chamber) by gravity. At the bottom of the condensation chamber, there was an outlet to collect the condensed water. A 0.45 µm PVDF membrane with the permeate side coated with carbon black NPs was given a tubular shape so that the diameter and length of the membrane tube was 16 mm and 50 mm, respectively. Distance between the outer surface (i.e., the permeate side) of the membrane tube and the inner surface of the PMMA tube was 27 mm. The bottom of membrane tube rested on the grooved center of a 1/2 inch-thick PMMA support which was slightly larger than the diameter of the membrane tube and had four legs connecting to the inner surface of the tubular system. Below this PMMA support, a small transparent container (Fig. 2) was placed in case there was any leaking of feedwater from the membrane tube. However, no leaking of feedwater was observed during experiments under natural sunlight when the systems were placed vertically.

Development of the three-stage planar permeate-side-heated solar membrane distillation system

The three-stage planar system was developed using transparent PMMA sheets (thickness: 1/8 or 1/2 inch). Each stage had a feedwater chamber [120 mm (L) × 50 mm (W) × 14 mm (H)], a transparent distillation chamber [the upper distillation chamber above the flange: 130 mm (L) × 60 mm (W) × 40 mm (H); the lower distillation chamber within the flange: 120 mm (L) × 50 mm (W) × 14 mm (H)], and a condensation chamber [150 mm (L) × 60 mm (W) × 30 mm (H)]. A 0.45 µm PVDF membrane was placed between distillation and feedwater chambers, with the permeate side of the membrane coated with carbon black NPs. The condensation chambers were covered by an aluminized heat barrier to keep the chamber cool. Two rubber gaskets (Grainger, Item No. 1MWF2) were cut and placed between the distillation chamber and the feedwater chamber, with the 0.45 µm PVDF membrane between these two rubber gaskets. In order to prevent leaking of feedwater and the loss of water vapor, these two rubber gaskets were pressed against each other with the help of screws and nuts. A copper sheet served as both the upper part of the condensation chamber and the bottom part of the feedwater chamber of the two adjacent stages (Fig. 5).

Single-stage planar permeate-side-heated solar membrane distillation systems

Two different types of single-stage planar systems were used when compared with the tubular and three-stage planar systems. The system used to compare with the tubular system had a 50 mm × 50 mm membrane, a feedwater chamber of 50 mm (L) × 50 mm (W) × 14 mm (H), a transparent distillation chamber [the upper part: 60 mm (L) × 60 mm (W) × 40 mm (H); the lower part within the flange: 50 mm (L) × 50 mm (W) × 14 mm (H)], and a condensation chamber of 207 mm (L) × 60 mm (W) × 30 mm (H).

The system used to compare with the three-stage planar system had a 120 mm (L) × 50 mm (W) membrane, a feedwater chamber of 120 mm (L) × 50 mm (W) × 14 mm (H), a transparent distillation chamber [the upper part: 130 mm (L) × 60 mm (W) × 40 mm (H); the lower part within the flange: 120 mm (L) × 50 mm (W) × 14 mm (H)], and a condensation chamber of 150 mm (L) × 60 mm (W) × 30 mm (H). These single-stage planar systems had no copper sheet.

Distillation experiments under natural sunlight

All the distillation experiments reported in this study were conducted under natural sunlight from sunrise to sunset. Most experiments were performed on the roof of Breezeway, FAU (26°22′19″N and 80°06′11″W), and only one experiment (the one at an average daytime irradiance of 613 W m^{-2}) was conducted at Spanish Oaks of Condominium (26°21′28″N and 80°5′58″W). The planar (both single-stage and three-stage) systems were tilted at 30° with respect to the horizontal in most experiments, while the tubular systems and the planar systems shown in Supplementary Fig. 1a were placed vertically (i.e., at 90° inclination). The systems were placed properly just before sunrise and the pyranometer (Hukseflux, LP02-LI19) was also set along with the systems to measure the irradiance of sunlight every 30 seconds. At the time of sunrise, all the feedwater reservoirs of the systems were filled with feedwater (i.e., DI water), and the hydrostatic pressure at the center of the membrane, exerted by the feedwater in the reservoir, was observed and recorded throughout the whole day. In order to maintain a steady hydrostatic pressure, feedwater was added every 2 h to the reservoirs to keep the water level steady. The temperature of feedwater in the reservoir was also recorded using a thermometer every 2 h during the experiments. The experiments were stopped right after sunset. Distilled water was collected from the condensation chambers after sunset, and weighed using an analytical balance (LF 224 R, Intelligent Weighing Technology) to calculate the distillate production rate per unit area of the membrane (i.e., distillate flux). Both the planar and tubular systems were also tested during the night from sunset to sunrise. However, no distilled water was produced during the night.

Footprint calculation

For the single-stage tubular system, the outer radius of the system was 0.038 m. Thus, the circular footprint of the tubular system was 0.0045 m^2 when placed vertically. For the single-stage planar system with the 50 mm × 50 mm membrane, the length of this system was 0.273 m and the width was 0.067 m. Hence, the footprint of this single-stage system was 0.016 m^2 (i.e., 0.067 m × 0.236 m) when placed at 30° inclination to the ground. For the single-stage planar system with the 120 mm (L) × 50 mm (W) membrane, the length was 0.283 m and the width was 0.067 m. Thus, the footprint of this single-stage planar system was also 0.016 m^2 (i.e., 0.067 m × 0.245 m) at 30° inclination to the horizontal. For the three-stage planar system, the length of footprint was 0.51 m when placed at 30° inclination to the ground and the width was 0.067 m. So the footprint of the three-stage system was 0.034 m^2 (i.e., 0.51 m × 0.067 m). Flanges were not considered in the footprint calculation of planar systems as flanges may not be used in real-world applications.

DATA AVAILABILITY

The datasets generated during and/or analyzed during the current study are available from the corresponding author on reasonable request.

REFERENCES

1. Eliasson, J. The rising pressure of global water shortages. *Nature* **517**, 6 (2015).
2. Schwarzenbach, R. P., Egli, T., Hofstetter, T. B., Von Gunten, U. & Wehrli, B. Global water pollution and human health. *Annu. Rev. Environ. Resour.* **35**, 109–136 (2010).
3. Pruss-Ustun, A. & Organization, W. H. *Safer water, better health: costs, benefits and sustainability of interventions to protect and promote health.* (World Health Organization, 2008).
4. Rundblad, G., Knapton, O. & Hunter, P. R. Communication, perception and behaviour during a natural disaster involving a 'Do Not Drink' and a subsequent 'Boil Water' notice: a postal questionnaire study. *BMC Public Health* **10**, 1–12 (2010).
5. Siembieda, W., Johnson, L. & Franco, G. Rebuild fast but rebuild better: Chile's initial recovery following the 27 February 2010 earthquake and tsunami. *Earthq. Spectra* **28**, 621–641 (2012).
6. Rudnick, H., Mocarquer, S., Andrade, E., Vuchetich, E. & Miquel, P. Disaster management. *IEEE Power Energy Mag.* **9**, 37–45 (2011).
7. Dai, Y., Huang, H. & Wang, R. Case study of solar chimney power plants in Northwestern regions of China. *Renew. Energy* **28**, 1295–1304 (2003).
8. Marston, L. et al. Reducing water scarcity by improving water productivity in the United States. *Environ. Res. Lett.* **15**, 094033 (2020).
9. Alam, K. Farmers' adaptation to water scarcity in drought-prone environments: a case study of Rajshahi District, Bangladesh. *Agric. Water Manag.* **148**, 196–206, https://doi.org/10.1016/j.agwat.2014.10.011 (2015).
10. Amankwah-Amoah, J. Solar energy in sub-Saharan Africa: the challenges and opportunities of technological leapfrogging. *Thunderbird Int. Bus. Rev.* **57**, 15–31 (2015).
11. Zeng, Y. et al. Solar evaporation enhancement using floating light-absorbing magnetic particles. *Energy Environ. Sci.* **4**, 4074–4078 (2011).
12. Ghasemi, H. et al. Solar steam generation by heat localization. *Nat. Commun.* **5**, 4449 (2014).
13. Ying, P. et al. Band gap engineering in an efficient solar-driven interfacial evaporation system. *ACS Appl. Mater. Interfaces* **12**, 32880–32887 (2020).
14. Xu, Y. et al. A simple and universal strategy to deposit Ag/polypyrrole on various substrates for enhanced interfacial solar evaporation and antibacterial activity. *Chem. Eng. J.* **384**, 123379 (2020).
15. Yang, L. et al. Marine biomass-derived composite aerogels for efficient and durable solar-driven interfacial evaporation and desalination. *Chem. Eng. J.* **417**, 128051 (2021).
16. Kim, M. et al. Laser-induced photothermal generation of flexible and salt-resistant monolithic bilayer membranes for efficient solar desalination. *Carbon* **164**, 349–356 (2020).
17. Li, Z. et al. Broadband-absorbing WO_{3-x} nanorod-decorated wood evaporator for highly efficient solar-driven interfacial steam generation. *Sol. Energy Mater. Sol. Cells* **205**, 110254 (2020).
18. Li, L., Hu, T., Li, A. & Zhang, J. Electrically conductive carbon aerogels with high salt-resistance for efficient solar-driven interfacial evaporation. *ACS Appl. Mater. Interfaces* **12**, 32143–32153 (2020).
19. Lou, J. et al. Bioinspired multifunctional paper-based rGO composites for solar-driven clean water generation. *Acs Appl Mater. Inter* **8**, 14628–14636 (2016).
20. Zhang, L., Tang, B., Wu, J., Li, R. & Wang, P. Hydrophobic light-to-heat conversion membranes with self-healing ability for interfacial solar heating. *Adv. Mater.* **27**, 4889–4894 (2015).
21. Zhu, L., Gao, M., Peh, C. K. N., Wang, X. & Ho, G. W. Self-contained monolithic carbon sponges for solar-driven interfacial water evaporation distillation and electricity generation. *Adv. Energy Mater.* **8**, 1702149 (2018).
22. Du, C. & Huang, C. A floating vapor condensation structure in a heat-localized solar evaporation system for facile solar desalination. *Appl. Therm. Eng.* **201**, 117834 (2021).
23. Ni, G. et al. A salt-rejecting floating solar still for low-cost desalination. *Energy Environ. Sci.* **11**, 1510–1519 (2018).
24. Tanvir, R. U., Sujon, S. A. & Yi, P. Passive permeate-side-heated solar thermal membrane distillation: extracting potable water from seawater, surface water, and municipal wastewater at high single-stage solar efficiencies. *ACS EST Eng.* **1**, 770–779 (2021).
25. Politano, A. et al. Photothermal membrane distillation for seawater desalination. *Adv. Mater.* **29**, 1603504 (2017).
26. Dongare, P. D. et al. Nanophotonics-enabled solar membrane distillation for off-grid water purification. *Proc. Natl Acad. Sci. USA* **114**, 6936–6941 (2017).
27. Zhang, Y. et al. Titanium nitride nanoparticle embedded membrane for photo-thermal membrane distillation. *Chemosphere* **256**, 127053 (2020).
28. Wu, X., Jiang, Q., Ghim, D., Singamaneni, S. & Jun, Y.-S. Localized heating with a photothermal polydopamine coating facilitates a novel membrane distillation process. *J. Mater. Chem. A* **6**, 18799–18807 (2018).
29. Wu, X. et al. A thermally engineered polydopamine and bacterial nanocellulose bilayer membrane for photothermal membrane distillation with bactericidal capability. *Nano Energy* **79**, 105353 (2021).
30. Huang, J., Hu, Y., Bai, Y., He, Y. & Zhu, J. Novel solar membrane distillation enabled by a PDMS/CNT/PVDF membrane with localized heating. *Desalination* **489**, 114529 (2020).
31. Kirkham, M. B. *Principles of Soil and Plant Water Relations*. 27–40 (2005).
32. Weidenfeller, B., Höfer, M. & Schilling, F. R. Thermal conductivity, thermal diffusivity, and specific heat capacity of particle filled polypropylene. *Compos. Part A: Appl. Sci. Manuf.* **35**, 423–429 (2004).
33. Jéquier, E. & Constant, F. Water as an essential nutrient: the physiological basis of hydration. *Eur. J. Clin. Nutr.* **64**, 115–123 (2010).
34. Sawka, M. N., Cheuvront, S. N. & Carter, R. 3rd Human water needs. *Nutr. Rev.* **63**, S30–S39 (2005).
35. Amin, M. A., Mahmud, K., Hosen, S. & Islam, M. A. In *4th Annual Paper Meet and 1st Civil Engineering Congress* (Dhaka, Bangladesh, 2011).
36. Arouna, A. & Dabbert, S. Determinants of domestic water use by rural households without access to private improved water sources in benin: a seemingly unrelated tobit approach. *Water Resour. Manag.* **24**, 1381–1398 (2010).
37. Fan, L., Liu, G., Wang, F., Geissen, V. & Ritsema, C. J. Factors affecting domestic water consumption in rural households upon access to improved water supply: insights from the Wei River Basin, China. *PLoS One* **8**, e71977 (2013).
38. Singh, O. & Turkiya, S. A survey of household domestic water consumption patterns in rural semi-arid village, India. *GeoJournal* **78**, 777–790 (2013).
39. Inman, D. & Jeffrey, P. A review of residential water conservation tool performance and influences on implementation effectiveness. *Urban Water J.* **3**, 127–143 (2006).
40. Willis, R. M., Stewart, R. A., Panuwatwanich, K., Williams, P. R. & Hollingsworth, A. L. Quantifying the influence of environmental and water conservation attitudes on household end use water consumption. *J. Environ. Manag.* **92**, 1996–2009 (2011).
41. Guan, G., Lou, H., Yao, C., Li, J. & Yang, X. Achieving sustainable operation for hypersaline membrane distillation applications: a novel strategy based on the critical Reynolds number. *Desalination* **499**, 114833 (2021).

AUTHOR CONTRIBUTIONS
S.A.S.: methodology, validation, formal analysis, investigation, writing–original draft, visualization. P.Y.: conceptualization, methodology, validation, formal analysis, data curation, writing–original draft, writing–review & editing, visualization, supervision, project administration.

COMPETING INTERESTS
The authors declare no competing non-financial interests but the following competing financial interests: patent applications have been filed for various passive permeate-side-heated solar membrane distillation systems.

ADDITIONAL INFORMATION
Supplementary information The online version contains supplementary material available at https://doi.org/10.1038/s41545-022-00192-z.

Correspondence and requests for materials should be addressed to Peng Yi.

Reprints and permission information is available at http://www.nature.com/reprints